ABSTRACT

There two common methods dealing with interpreting data from infrared thermography: qualitatively and quantitatively. On a certain condition, the first method would be sufficient, but for an accurate interpretation, one should undergo the second one. This report proposes a method to estimate the defect depth quantitatively at an inner wall of petrochemical furnace wall. Finite element method (FEM) is used to model multilayer walls and to simulate temperature distribution due to the existence of the defect. Five informative parameters are proposed for depth estimation purpose. These parameters are the maximum temperature over the defect area ($T_{max\text{-}def}$), the average temperature at the right edge of the defect ($T_{avg\text{-}right}$), the average temperature at the left edge of the defect ($T_{avg\text{-}left}$), the average temperature at the top edge of the defect ($T_{avg\text{-}top}$), and the average temperature over the sound area ($T_{avg\text{-}so}$). Artificial Neural Network (ANN) was trained with these parameters for estimating the defect depth. Two ANN architectures, Multi Layer Perceptron (MLP) and Radial Basis Function (RBF) network were trained for various defect depths. ANNs were used to estimate the controlled and testing data. The result shows that 100% accuracy of depth estimation was achieved for the controlled data. For the testing data, the accuracy was above 90% for the MLP network and above 80% for the RBF network. The results showed that the proposed informative parameters are useful for the estimation of defect depth and it is also clear that ANN can be used for quantitative interpretation of thermography data.

ABSTRAK

Ada dua kaedah umum berkenaan dengan pengolahan data daripada termografi infra merah: secara kualitatif dan secara kuantitatif. Pada keadaan tertentu, kaedah pertama sudah mencukupi, tetapi untuk interpretasi yang tepat, kaedah kedua perlu digunakan. Lapuran ini mencadangkan kaedah untuk menganggar kedalaman kerosakan yang berada pada dinding sebelah dalam ketuhar petrokimia secara kuantitatif. Metod elemen terbatas (FEM) digunakan untuk pemodelan dinding banyak lapis dan untuk mensimulasikan taburan suhu yang terbentuk disebabkan kerosakan pada dinding dalaman. Lima parameter informatif dicadangkan untuk pengiraan kedalaman kerosakan. Parameter ini adalah suhu maksima pada kawasan kerosakan ($T_{max\text{-}def}$), suhu purata pada sisi kanan kerosakan ($T_{avg\text{-}right}$), suhu purata pada sisi kiri kerosakan ($T_{avg\text{-}left}$), susu purata pada sisi atas kerosakan ($T_{avg\text{-}top}$), dan suhu purata pada kawasan yang tidak rosak ($T_{avg\text{-}so}$). Rangkaian neural buatan (ANN) telah dilatih menggunakan parameter ini untuk pengiraan kedalaman kerosakan. Dua rangkaian neural *Multi Layer Perceptron* (MLP) dan *Radial Basis Function* (RBF) telah dilatih menggunakan pelbagai macam kedalaman kerosakan. ANN digunakan untuk mengira data kawalan dan data ujian. Hasil menunjukkan 100% ketepatan penganggaran kedalaman telah dicapai untuk data kawalan. Untuk data-data ujian, ketepatan adalah melebihi 90% untuk rangkaian neural MLP dan 80% untuk rangkaian neural RBF. Hasil ini membuktikan bahawa informatif parameter yang dicadangkan adalah berguna untuk pengiraan kedalaman kerosakan dan juga menunjukkan bahawa rangkaian neural dapat digunakan untuk interpretasi data termografi secara kuantitatif.

TABLE OF CONTENTS

GLOSSARY OF FIGURES

GLOSSARY OF TABLES

ACKNOWLEDGMENT

All praises to the Sustainer of the worlds, the Creator of the universe and all of its content. Grace, honor, and salutations on the Chief of Apostles, Muhammad (PBUH), his family, and companions.

I would like to take this moment to express my deepest thank to my PhD student, Mr. Rudi Heriansyah who has relentless worked very hard together to complete this undertaken project.

Also I would like to express my gratitude to other member of Computer Vision, Video, and Image Processing (CVVIP) Lab., Dr. Musa Mohd Mokji and Dr. Usman Ullah Sheikh for their supports, and suggestions in making this project a successful one.

Also, I wish to thank the government of Malaysia for supporting this research via Ministry of Higher Education (MOHE) and Research Management Centre (RMC) through grant: 78120 for supporting this project. Even though the amount was not that much but it surely helped in completing this project

CHAPTER 1

INTRODUCTION

1.1 Background

Infrared thermography (IRT) (Kaplan, 1993), (Maldague, 1993), (Gaussorgues, 1994), (Maldague, 2001) is one of many existing nondestructive testing techniques for preventive (PM) or predictive maintenance (PdM) (Mobley, 1990), (Gardner, 1992), (Levitt, 2003). Among others, the popularity of IRT lies in its contactless, easy to interpret the thermal data, large area of inspection, and free from dangerous radiation.

In the last few decades, IRT has gained much attention and has been successfully applied to the areas of electrical, mechanical, petrochemical, building and structures, material testing, industry, medical, and many others various applications (Kaplan, 1993) ranging from breast cancer detection (Qi *et al.*, 2002) to SARS (severe acute respiratory syndrome) diagnosis (Wang *et al.*, 2004), from aircraft inspection (D'Orazio *et al.*, 2005) to buildings application (Lo and Choi, 2004).

1.1.1 Thermal Image

The output data from IRT is temperature values which can also be viewed in an image form. This image is commonly known as *thermal image* or *thermogram*. Thermal image is captured using an *infrared thermal camera* or simply *thermal camera* (not to confuse with an *infrared camera* which is commonly applied for a night vision application). Essentially this device captures electromagnetic spectrum within infrared bands (0.78 – 1000 μm) (Figure 1.1). Therefore, unlike the intensity

image which lies within the visible light, a thermal image is a function of radiated energy of an inspected object (Kaplan, 1993).

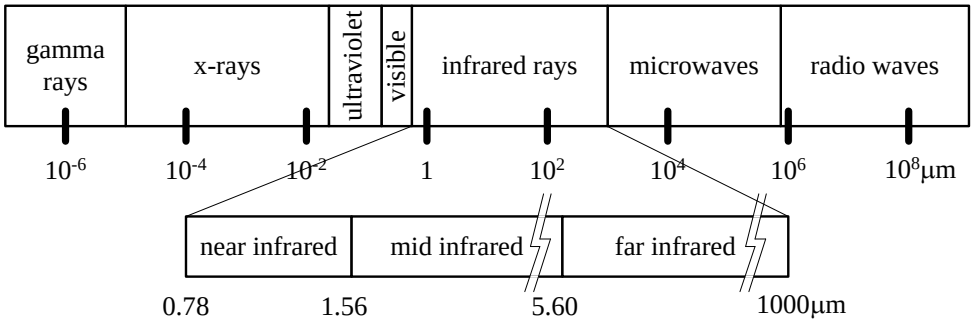

Figure 1.1 Electromagnetic spectrum

According to its working wavelength, thermal camera can be divided into two groups: *short wave* and *long wave* thermal cameras. A short wave (SW) camera operates in bands between 3 and 5 μm and a long wave (LW) camera operates in bands between 8 and 12 μm. The LW camera is of particular interest for measuring radiation from objects at room temperature (an example is for the detection of intruders by law enforcement agencies). The SW camera is best suited for warmer objects (an example is any process releasing CO_2, such as combustion engines) (Maldague, 2001).

Raw data captured by a thermal camera is in the form of temperature values. Thermal camera manufacturers usually have their own software to read this data and display them as a thermal image. When converting temperature values into thermal image, a *pseudo-coloring* or *false-coloring* technique (Chanda and Majumder, 2000) is used.

Certain color level represents certain temperature values. In the software terminology, this color map is called *palette*. IRBIS and IRBIS Plus V2.2 (from InfraTec GmbH Dresden) has seven palettes: *varioscan*, *varioscan printer*, *black → white*, *white → black*, *iron*, *blue → red*, and *stufen*. While ThermaCAM Explorer 99 (from FLIR Systems) offers more various palettes: *glowbow*, *grey*, *grey10*, *greyred*, *iron*, *iron10*, *medical*, *midgreen*, *midgrey*, *rain*, *rain100*, *rain900*,

and *yellow*. Figure 1.2 shows a visible image along with its thermal image in several palettes from ThermaCAM Explorer 99.

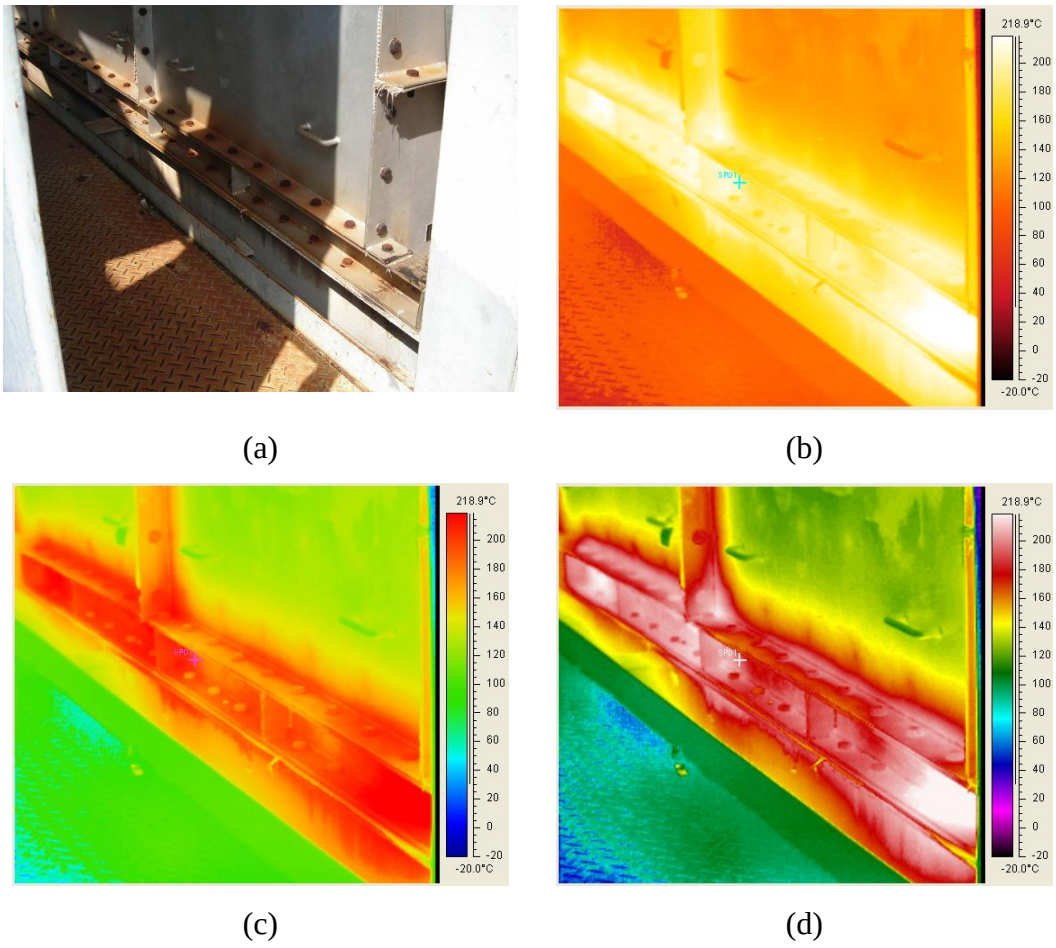

Figure 1.2 (a) Visible image with its thermal image (b) *glowbow*, (c) *midgreen* and (d) *rain* palette

1.1.2 IRT Inspection Modes

Based on how the thermogram is produced, there are two types of IRT: *active* and *passive* thermography. In active thermography, an external heat source is applied when capturing thermogram. One common heat source is a flash lamp or pulse generator. In a normal condition, the temperature gradient between the defective and nondefective (sound) area is undistinguishable. Immediately after applying the heat flash, the infrared thermal camera can record the difference between these two areas. In passive thermography, no external heat source is applied when capturing the

thermogram since the temperature difference between defective and sound area is so obvious already. Passive thermography is usually employed to a hot inspected object. Figure 1.3 shows configuration for these two modes of IRT.

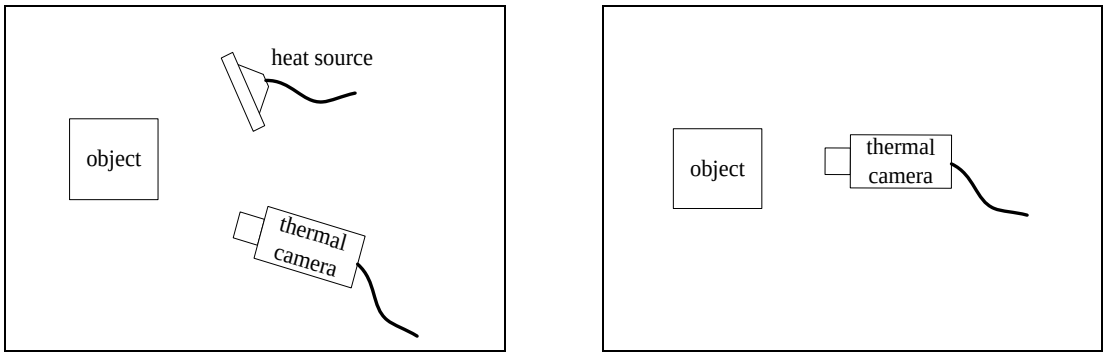

(a) (b)

Figure 1.3 IRT modes: (a) active thermography, (b) passive thermography

1.1.3 IRT Applications in Petrochemical Industries

One area where IRT has played an important role is in the petrochemical industries. This type of industry is categorized as a heavyweight industry with high investment cost, operational cost, and maintenance cost, along with high requirement for safety. Any problem found in running facilities should be detected earlier since breakdown of equipment will affect other equipments or even the entire operation of the plant. Maintenance should be scheduled properly and regularly because shutdown or startup equipment cannot be done suddenly as it is related to operational cost. Petrochemical site is a hazardous area, therefore entering this site should adhere to the safety standard. Because of these conditions the PdM and nondestructive evaluation (NDE) technique using IRT with its remote access capability have more advantageous over other PdM schemes.

Several big petrochemical industry players such as BP Amoco (Nyholt, 2000), Texaco (Ohliger and Alvarado, 2001) and Chevron Texaco (Ohliger, 2002) have taken the benefit of IRT technology. One example of a local petrochemical company that uses this technology in its predictive maintenance program is MTBE Malaysia Sdn. Bhd., located at Gebeng, Kuantan, Pahang, Malaysia. IRT inspection

in this company is still engaged by the third party service company. All thermal images used in this thesis have been provided by the courtesy of MTBE.

Some other applications of IRT in petrochemical industries, refineries, or facilities are in the inspection of tanks (Sims, 2001), boilers (May, 2003), process vessels (Bonin, 2003), horsehead (beam) pump (Ohliger, 2003), lagged pipe (Willis, 2004), furnace tube (LeClercq, 2003), refractory lined petroleum refinery equipment (Whitcher, 2004), and process heaters (Weigle, 2005). These various applications proved that IRT is a suitable tool for petrochemical industry inspection.

1.1.4 Refractory Lined Equipments

Among inspections done in the petrochemical industries, inspection of refractory lined equipments is one of the popular applications of IRT. This is a passive thermography application. Pipes (Whitcher, 2004), cracking furnace (Weigle, 2005), boiler and incinerator are the equipments that use refractory materials in their construction. Figure 1.4, 1.5, and 1.6 show the visible images and their thermograms for the cracking furnace, boiler, and incinerator respectively.

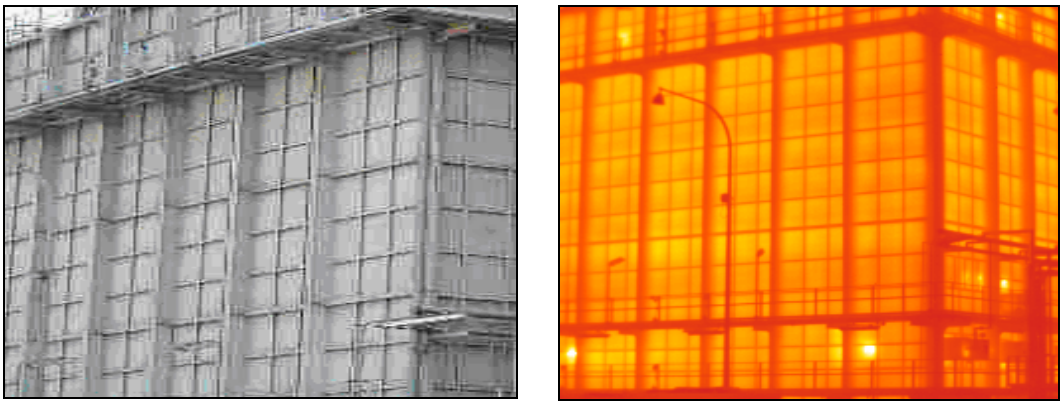

(a) (b)

Figure 1.4 (a) Cracking furnace and (b) its thermogram

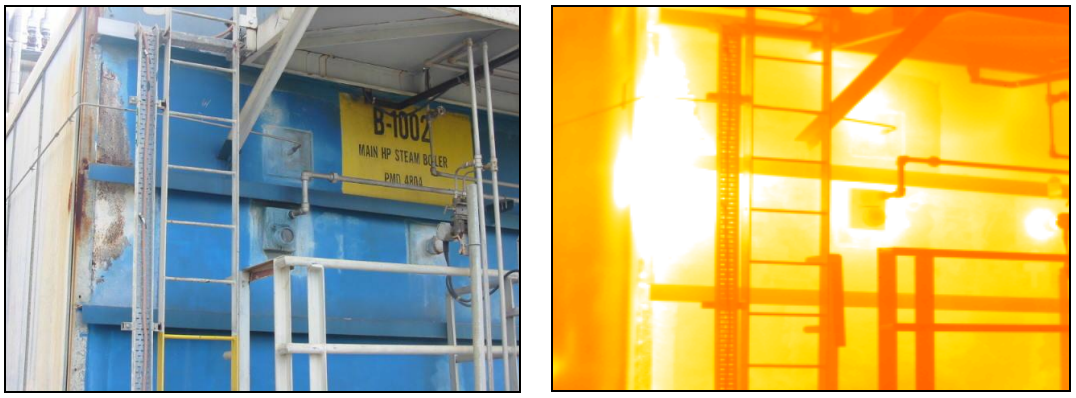

(a) (b)

Figure 1.5 (a) Defective refractory boiler and (b) its thermogram

(a) (b)

Figure 1.6 (a) Defective refractory incinerator and (b) its thermogram

1.1.5 Refractory Materials

Refractories are a family of technical ceramics. They manage industrial process heat, defying thermal and mechanical abuse and high temperature chemical attack (Carniglia and Barna, 1992). Refractories are stable materials that retain their strength at high temperatures, have resistance to abrasion and to furnace gases, and have poor thermal conductivity (good heat-insulating capacity) (Trinks *et al.*, 2004). The commonest duty of refractory is to contain high temperatures: to erect a solid barrier between hot *inside* and ambient tolerable *outside* (Carniglia and Barna, 1992).

Furnace walls are built from insulating refractories and encased in a steel shell to reduce flow of heat to the surroundings, and loss is further reduced by the

insertion of fiber block between the insulation refractories and the steel casing (Trinks *et al.*, 2004).

Modern firebrick (from fireclay, kaolin) and silica brick are available in many compositions and many shapes for a wide range of applications and to meet varying temperature and usage requirements. High-density, double-burned, and super-duty (low-silica) firebrick have high-temperature heat resistance, but relatively high heat loss. Thus they are usually backed by a lower density insulating brick.

1.1.5.1 Monolithic Refractory

Monolithic refractories are classified by physical properties, consistencies, and grain sizing (e.g., powder, paste, clay). Construction methods have been developed to suit various installation procedures such as pouring, troweling, gunning, ramming, patching, blowing, slinging, vibrating, spraying, foaming, or injecting. The castable (poured), plastic (rammed), or blown (sprayed, foamed) forms of refractory materials are generally superior to layed-up, dipped refractory brick construction because they are less prone to leak, and they provide extended furnace life (Griswold, 1946), (Chesters, 1973).

Monolithic refractories can be transferred by pumps over long distances and in large quantities for pouring in position. Because the weight of monolithic refractory in a furnace is held by a large number of supports, small or large areas can be repaired or replaced wherever necessary without affecting the surrounding area. Monolithic refractory materials adhere well to surrounding materials.

Monolithic refractories are suitable for walls that must be gas tight. The weight of the furnace itself is sustained by supports that help the monolithic material adhere to the shell and prevent gas leakage.

Monolithic refractories have lower thermal expansion than most refractory bricks. Whatever small expansion does occur can usually be absorbed by the supports. Therefore, unlike refractory bricks, monolithic refractory walls do not require clearances for thermal expansion. Clearances required for brick construction may allow passage for furnace gas leaks out or air into a furnace. The superior

sealing capability and reduced expansion of monolithic refractories make them suitable for higher furnace pressures and temperatures. Among the reasons for the growing use of monolithic refractories are versatility of the material and the flexibility of the self-supporting anchor system (Carniglia and Barna, 1992).

1.1.5.2 Fiber Refractory

Refractory materials can be melted, spun, and blown into fiber strands similar to ‘wool’ or ‘blanket’ insulations. They are used in many medium- and low-temperature furnaces and oven furnaces, and for outer layers in multilayered refractory walls. Because of all their small air spaces, they are much better insulators than solid refractories, but they are more fragile, less durable, and more difficult to install so that they do not settle, shrink, or otherwise lose their good insulating property (Carniglia and Barna, 1992).

1.1.6 Refractory Fail

At very high temperature, refractory become more and more porous, allowing the hot materials inside to attack the chemistry of the refractory. Over the time, this attack reduces the surface strength of the refractory and causes their melting temperatures to be lowered which may then cause the *spalling*. Spalling is defined as the breaking or cracking of refractory brick in service, to such an extent that pieces are separated or fall away, leaving new surfaces of the brick exposed (Griswold, 1946).

In Figure 1.5 and 1.6, the defective area or hot spots are indicated with bright color in thermogram. The hot spot temperature in Figure 1.5(b) is around 264.4^{o}C, and in Figure 1.6(b) is around 300.0^{o}C. As reported (MTBE, 2007), these temperatures are very critical and signs to refractory failure. These cracks will make the heat loss by conduction through the furnace walls and then by radiation and convection from outside furnace surface, in which may have a significant effect on the furnace economy (Trinks *et al.*, 2004).

Another unwanted possibility is the *refractory failure* which can cause catastrophic equipment damage, unscheduled or early turn-around and pose serious safety concerns for employees. By considering all these possibilities, it is critical to know current condition of the furnace walls and early warning of refractory breakdown indicated by hotspot or abnormal temperature distribution at certain location (Trinks *et al.*, 2004).

1.1.7 Heat Loss from Wall Surface

Refractory walls are frequently constructed from two or more layers of brick through which heat flows in series, escaping to the outer surface by convection and radiation. Figure 1.7 shows common wall layers for a boiler. In the modern boiler wall, layers 1 and 2 are usually composed of fiber blanket materials.

Besides thickness, the thermal conductivities of the component layers of brick, surface temperatures, and surface coefficients of convection and radiation are all interrelated with heat loss (Griswold, 1946), (Doležal, 1961). Both convection and radiation coefficients increase with temperature, radiation more rapidly (Cone, 1980).

Convection heat losses occur when furnace gases exit around doors/peepholes and through crack or dropout load discharge chutes, sometimes burning as they go but always carrying away heat. This kind of losses may involve cold air leaking into a furnace as well as hot gases leaking out. The losses from cold air in-leakage are usually larger than those from hot gas out-leakage. Cold air in-leakage occurs if the opening is at a level where the pressure inside the furnace is less than the pressure outside at the same elevation, thus sucking ‘tramp air’ (excess air) into the furnace through any cracks or openings. This cold air in-leakage may chill some of the load pieces, turning them into rejects, or else requiring a longer heating cycle to achieve good temperature uniformity, and therefore using more fuel (Trinks *et al.*, 2004).

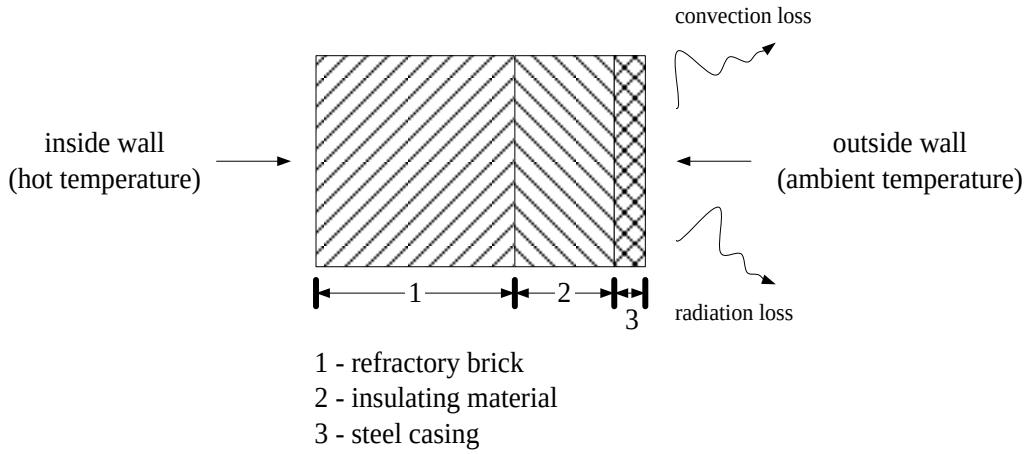

Figure 1.7 Boiler wall layers

1.2 Motivation

In IRT technology, thermal data or thermal image (thermogram) is the main output. In the current practice, the interpretation of the thermal image in most petrochemical applications is done manually by human operator. Most of the data are analyzed qualitatively by human vision system. This report thus proposes an automatic way for interpreting the thermogram from refractory lined equipments or facilities in term of defect depth estimation.

1.3 Objective

The objective of this work is to simulate the temperature behavior on the front wall due to the existence of back wall defect and to develop an algorithm that can automatically estimate the defect depth as depicted in thermal images. Artificial neural network is used for this purpose. For verification purpose, the developed algorithm and its implementation are tested with trained and untrained data.

1.4 Scope of Work

This work is limited to the following scopes:

- Thermal data used is in the form of temperature values for defect characterization.
- Thermal image is obtained from passive thermography scheme meaning that no time dependency from one thermal image to another, hence no thermal contrast computation is needed.
- Defect to be modeled and analyzed will be spalling defect.

1.5 Report Organization

The report is organized as follows. Chapter 2 reviews some existing technique for defect depth estimation for infrared thermography applications. Chapter 3 discusses the numerical modeling for passive thermography for the use of defect simulation and temperature behavior study. The proposed informative parameters are discussed as well. Experimental results for each of the proposed techniques for verification purposes are presented in Chapter 4. The last Chapter 5 summarizes and concludes the report and gives recommendation for future work.

CHAPTER 2

LITERATURE REVIEW

2.1 Overview

This chapter discusses the current trend of infrared thermography (IRT) applications. The existing methods for numerical modeling of IRT-based approach and defect detections and characterizations are reviewed. The proposed method for defect characterization in passive thermography application is briefly described as well.

2.2 Numerical Modeling in IRT

In IRT, numerical modeling is a precious tool. It can provide limits to the effectiveness of IRT technique and also the possibility of considering different defect geometries and determining their detectability without the expense of making and testing the corresponding specimens (James *et al.*, 1989).

Other purpose of numerical modeling in IRT is to simulate the real situation in order to obtain the simulated thermogram from that simulation (Conner, 1998). This thermogram can be used to test the developed algorithms (mainly related to image processing) in case of the unavailability of the thermogram from the real object, for instance due to the difficulties to obtain such thermal data.

From modeling tools perspective, there are two common methods for numerical modeling in IRT and these are the finite difference method (FDM) (Özişik, 1994), (Croft and Lilley, 1977) and the finite element method (FEM) (Segerlind, 1984), (Rao, 1989), (Kattan, 2003), (Lewis *et al.*, 2004), (Akin, 2005). FDM is simple and easy to implement but it fails when handling irregular geometry

or anisotropic materials. FEM although is quite complex it can work elegantly on deformed shapes and non-homogeneous materials (ElShayeb and Beng, 2000). In addition it also improves the accuracy and efficiency (Huebner *et al.*, 1995).

FEM has been successfully applied to simulate the real world problems. Sukirman (1994) used FEM for solving a fully coupled problem in petroleum reservoir engineering. Sabir and Mousa (1999) utilized FEM based on cylindrical and conical curved shell elements for analysis of storage tanks. Andreev and Harmuth (2003) simulated the thermo-mechanical behavior and failure of ceramic refractory materials for the lining furnaces and vessels of the steel industry. A simulation of the thermo-mechanical behavior of the refractory lining of a blast furnace was conducted by Gruber *et al.* (2004). Ghojel and Ibrahim (2004) simulated double-channel induction furnaces to study thermal stresses in the refractory lining. The simulation results showed a correlation between simulated data with actual data.

In IRT, the application of FEM is currently widely used. Although in the early years FDM was usually employed for heat behavior study (Buglia and Brinkworth, 1958), (Charles and Wilson, 1980), (Saintey and Almond, 1995), (Darabi, 2000). The trend in the last few years shows that FEM is a common alternative used by researchers (Chowdhury, 2004), (Krishnapillai *et al.*, 2005), (Krishnapillai *et al.*, 2006).

2.2.1 Numerical Modeling Tool

One can choose two alternatives when building the numerical model in IRT: firstly, by self-formulation of the model and then writing the computer codes for this model, or secondly by using existing commercial software available in the market.

Among existing commercial FEM software, COSMOSWorks™ (SRAC, 2004), (Kurowski, 2006) is one of the common tools used today for solving the field problems. Its advantage is laid on its visual appearance that can make the modeling task easier. Its integration with SolidWorks®, a design automation software, makes the modeling and simulation jobs more efficient and effective. This thesis takes the

advantages of these software packages for numerical modeling in passive thermography.

2.2.2 Informative Parameters in IRT

The informative parameters in thermography are any parameters that can be used to characterize the properties of subsurface defect based on their behaviour on the other side of the outer surface. These parameters can be a time constant or any magnitudes such as temperature values that can be related with the defect existence.

Most investigations for informative parameters derivation were devoted to active IRT. Saintey and Almond (1995) used 2-D FDM modelling to simulate the conductive heat flow containing a circular crack-like defect by means of transient thermography. It was shown that the thermal contrast and FWHM (full-width at half maximum) have relations with size, depth, thermal resistance, and material properties of defect.

Saintey and Almond (1997) also used five 'measurable' parameters to train artificial neural network for defect depth estimation. These informative parameters were the time image contrast reaches half its maximum, the time image contrast falls to half its maximum, image FWHM at half rise time, image FWHM at half fall time, and the maximum relative contrast attained by the image.

Plotnikov (1998) discovered that time of peak slope t_{ps} is an informative parameter for defect depth estimation. Other parameters such as the amplitude, phase, maximum thermal contrast (C_{max}), and the maximum time t_{max} (when C_{max} occurred) were also sensitive to depth variation. It was concluded that the amplitude and phase parameters have non-homogeneous character and were not applicable for defect depth extraction. This study was dedicated to transient thermography.

Plotnikov and Winfree (2000) focused their research on defect depth estimation in composite aircraft components using transient thermography. Four time parameters were studied: time when thermal contrast $C(t)$ crosses a specified threshold level t_{div}, time when the first derivative of thermal contrast reaches its maximum t_{ps}, time interval corresponding to the contrast reaching 0.72 of the

maximum contrast value t_{07}, and time when thermal contrast reaches its maximum t_{max}. It had been found that t_{div} and t_{ps} were approximately independent of flaw size for shallow defects and differed significantly only for deeper defects. In contrast, t_{max} and t_{07} have a large dependence on flaw size for shallow depths.

Maierhofer *et al.* (2004) did numerical simulation to study the influence of material and geometrical parameters on impulse thermography for buildings materials. Three parameters were studied: concrete cover, void size, and thermal properties of materials. These parameters influenced the thermal signature behaviour (maximum temperature difference), therefore they were informative parameters in this study.

Chowdhury (2004) used FEM to investigate the behavior of temperature in a concrete slab in term of impulse thermography. The defect was simulated as a large void. There were two 3-D models used in their study. The first model had length and width 0.50m and thickness of 0.20m. The void defect size was 0.10m long by 0.10m wide and by 0.10m thick. The voids were located at 2, 4, 6, and 8 cm from the top of the surface. The second model consisted of 1.0m long by 1.0m wide by 0.5m thick concrete slab. It had voids of 0.20m long by 0.20m wide by 0.20m thick and located at 2, 4, 6, 8cm from the top of the surface. Figure 2.1 shows these models. Heat flux was applied to the top surface. Adiabatic conditions were assumed for the other surface.

Their study had shown that the thermal signal ($\Delta T = T_{void} - T_{background}$) and contrast ($C = \frac{\Delta T}{\Delta T_{background}}$) were dependent on the void *size*, *thickness*, and *depth*. Another important issue shown from this result was that the numerical simulation result using FEM had good compromise with experimental results of the physical problem.

Krishnapillai *et al.* (2006) did FEM modeling in terms of pulse thermography to study composite subsurface defects. They showed that there were dependencies between defect depth, thickness, and size with the maximum temperature difference on the surface.

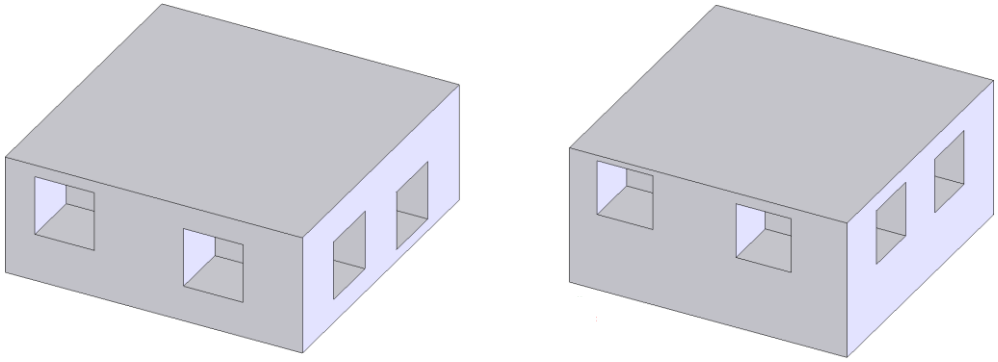

(a) (b)

Figure 2.1 Concrete slab: (a) first model, and (b) second model

2.3 Existing Defect Characterization Techniques

Few efforts have been made for defect characterization in infrared thermography. Based on literature survey up to this thesis writing, most of these efforts have been devoted for active thermography. Meaning that the temporal property (time) is one of the component that playing role for characterization purpose. But for defect sizing in passive thermography, only spatial properties are considered.

Almond and Lau (1994) proposed analytical treatment for defect sizing of mild steel by transient thermography. The full width at half-maximum (FWHM) was employed as a means of circular defect sizing (Figure 2.2). They suggested that for 10mm defect diameter, the following relation should be used: $\text{FWHM} = [10 - 1.08(\alpha t)^{1/2}]$ mm.

Saintey and Almond (1995) also recommended in using FWHM (Figure 2.2) for defect sizing in transient thermography. They showed that defect size has a relation with FWHM and confirmed that shallow defects have FWHMs that change more rapidly, and by a larger amount, than deeper defects. Sizing of such defects is therefore more difficult than might be imagined.

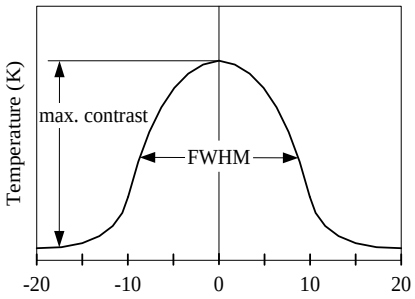

Figure 2.2 Schematic diagram of maximum contrast and FWHM along a line passing through the image center

Saintey and Almond (1997) employed ANN for characterization of defect *size* and *depth* from transient thermography data. The NN was trained on a comprehensive range of finite difference modeling results and is shown to provide a simple means of interpreting practical experimental measurements.

Numerical finite-difference modeling has been employed in a detailed investigation of spatial and temporal dependences of transient thermography images on defect size, depth and other parameters. The model was formulated in cylindrical polar coordinates, using the alternating direction implicit (ADI) technique (Croft and Lilley, 1977) for the solution of the resulting finite difference equations. The modeled crack defects were circular, and parallel to the surface of the material in which they were embedded. The crack defect was modeled in mild steel as a contact resistance between two layers of nodes.

Two parameters were studied: the *peak image contrast* and the *full-width at half maximum contrast* (FWHM), see Figure 2.2. They showed that defect *size* and *depth* have dependence on these two parameters. From here, they proposed the followings five ‘measurables’ as combination of image contrast, FWHM, and time: (1) the time image contrast reaches half its maximum value, (2) the time image contrast falls to half its maximum value, (3) image FWHM at half rise time, (4) image FWHM at half fall time, and (5) the maximum relative contrast attained by the image. NN with the architecture as shown in Figure 2.3 was used for training using *back-propagation* algorithm. They obtained average absolute error of 2.89% for defect size estimation and 2.34% for defect depth estimation.

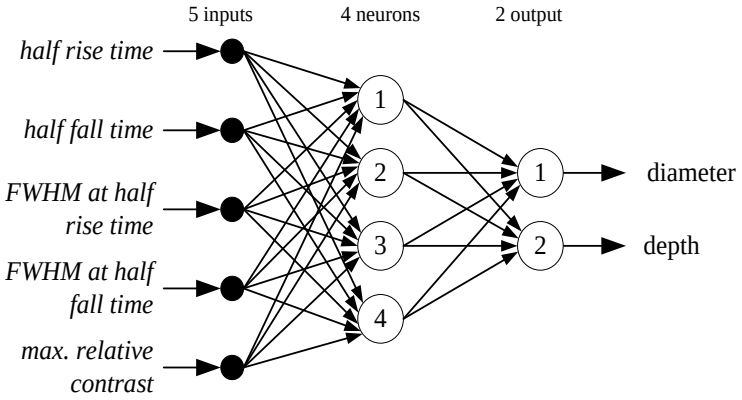

Figure 2.3 MLP-NN as size and depth estimator for mild steel material

Manduchi *et al*. (1997) used NN for defect characterization by means of a transient thermography. The normalized contrast $C(t) = \frac{T_d(t)}{T_d(t_{ref})} - \frac{T_s(t)}{T_s(t_{ref})}$ was selected for NN inputs. The input vectors for the NN are composed of the sampled values of triangular functions ranging from 0 (for x=0 and x=1) and 1 (for some x in the range [0,1]). A triangular function represents in fact a raw approximation of the time evolution of the normalized contrast. They proposed two NNs for this purpose. The first NN consists of 40 input units, 10 units in the hidden layer and a single output unit. The second NN consists of 40 input units, 30 units in the hidden layer, and 20 output units to produce a Gaussian function centered in the vertex position.

Plotnikov (1998) proposed the second partial derivative of the contrast $C^r(t) = \frac{T_{def}(t) - T_{soa}(t)}{T_{soa}(t)}$ to estimate the defect size, where T_{def} is temperature above the defect and T_{soa} is temperature above the defect free (sound) area. The parts of the contrast curve where $\frac{\partial^2 C}{\partial x^2} < 0$, define the size of the defects. For depth estimation in transient thermography, he investigated five informative parameters: the maximum value of the thermal contrast C_{max}, the when this maximum occurs t_{max}, the time of the peak slope t_{ps} of the thermal contrast curve, the amplitude, and the phase of the discrete Fourier transform of the temperature evolution after the heat injection. He concluded that t_{ps} is a steady characteristic for depth estimation and proposed this

property by taking square root of the time and this approach is limited to the depths less than a half of the plate thickness.

Maldague *et al.* (1998) studied defect depth using MLP-NN with back-propagation in pulsed phase thermography (PPT). NN with 32 inputs neurons, 8 neurons in the first hidden layer, 21 neurons in the second hidden layer, and 1 output neurons was used (Figure 2.4). The inputs were 32 phase values $\phi(f)$ of aluminum material. NN was trained with 0.04 to 10mm defect depth. It was observed that for depth smaller than 3mm, estimation error of NN is very high (100% error at 2.3mm depth).

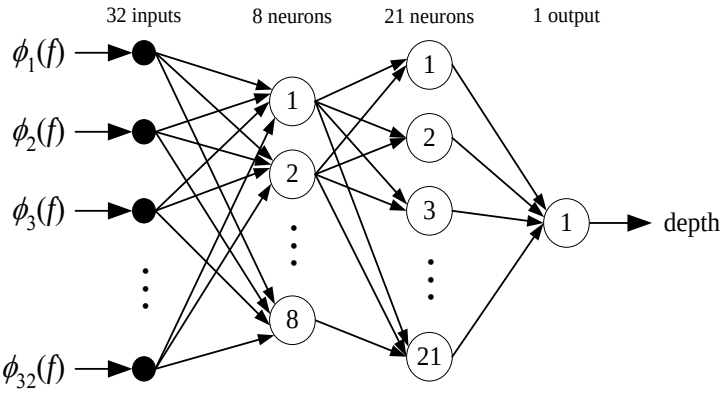

Figure 2.4 MLP-NN as depth estimator for aluminium material

Plotnikov and Winfree (2000) in their work for transient thermography studied *four* informative parameters for estimation of defect depth. The time when $C(t)$ crosses a specified threshold level t_{div}, the time when the contrast curve has the peak slope t_{ps}, the time when the thermal contrast reaches its maximum t_{max}, and the time interval corresponding to the contrast reaching 0.72 of the maximum contrast value t_{07}. To characterize the defect depth, the following relation was used: $d = a\sqrt{t_{char}} + b \cdot t_{char} + c$, where t_{char} is one of the temporal informative parameters and a, b, and c are predetermined constants. From their research also, some properties of t_{char} were studied. For example, it is difficult to obtain a depth profile based on t_{div} parameter for shallow (depth in less than 2mm) defects. The depth estimation based on t_{max} parameter has a noticeable crater-like surface for shallow defects. The deep (depth is greater than 6mm) defects cause noisy profiles estimated

from t_{ps}, while for other parameters, deep defects result in more rounded estimated profiles for the defect.

Darabi (2000) used ANFIS (Adaptive Network-based Fuzzy Inference System) (Jang *et al.*, 1997) for defect depth estimation. For training, seven informative parameters were used for inputs, i.e. half-rise contrast $-h_{C\max}$, maximum contrast $C_{\max}$, half-decay contrast $+h_{C\max}$, half-rise contrast time $t^{-}_{1/2C_{\max}}$ maximum contrast time, maximum contrast time $t_{C\max}$, and half-decay contrast time $t^{+}_{1/2C_{\max}}$. The output was the depth. Two bell-shape membership functions were assigned for each input, that made ANFIS had 64 rules. It was shown that ANFIS was able to estimate the depth, with error 8.66% (or 91.34% correct estimation).

Vallerand and Maldague (2000) proposed a method for characterization of defect thickness for aluminum corrosion using statistical processing method by means of pulsed infrared thermography (PIRT). This technique has two phases: *learning* and *analysis* phases. In the *learning phase*, the temperature images with known flaw including background (sound area) are obtained, and the mean and variance of these data are calculated. In the *analysis phase*, at each time step, the probability of each pixel being any of the known flaw or background is computed with Gaussian probability along with its means and variance. All probabilities of being a given known defect or background at each time step are multiplied together for obtaining the global probability of each pixel. The winning category corresponds to the largest probability value. This identifies the unknown pixel location as the more probable known flaw. They reported also that this statistical technique when using phase data had a better performance compared to perceptron and Kohonen neural network. They also showed that a better performance can be achieved if two-step method is used, e.g. flaw detection with phase data and flaw characterization with amplitude data.

Maldague (2001) used the gradient of the contrast image $C_{\max}$ for defect sizing. From this gradient image $|G|$, the defect shape was extracted. He showed the procedure to estimate the true size of the defect by calibrating each pixel size respect to the apparent size of field of view with the actual thermogram dimension.

Darabi and Maldague (2002) used simulated data from 3-D finite difference modeling to detect and to estimate the depth of the delamination defect of CFRP (carbon fiber reinforced plastic) material. The *running contrast* $C^r(t) = \frac{T_{def}(t) - T_{soa}(t)}{T_{soa}(t)}$ as proposed by Plotnikov (1998) was used to train NN for as defect detector and depth estimator. Thus, two different NNs were used for defect detection and depth estimation.

For defect detection, three layers MLP with 30 input neurons, 15 neurons in hidden layer, and 1 output neurons was used (Figure 2.5). This network was trained using 130 input-output pair vectors (105 input vectors were running contrast curves over defect areas and 25 were over sound area) extracted from the samples which contained air delamination defects at different depths and configurations. They claimed 96.8% of correct detection result for this network.

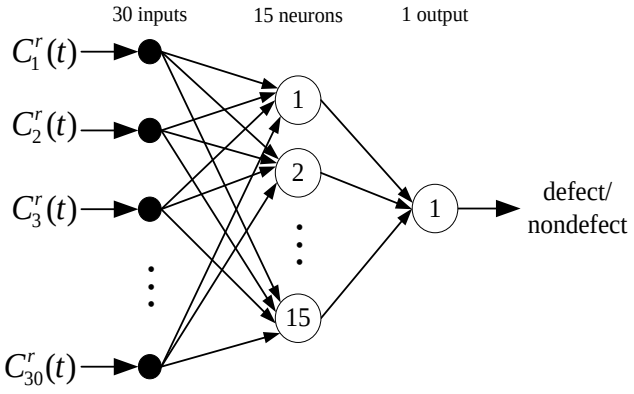

Figure 2.5 MLP-NN as defect detector for CFRP material

For defect detection, as before, three layers MLP (Figure 2.6) with 20 input neurons, 15 neurons in hidden layer, and 15 output neurons was trained using 140 input/output vectors. The input vectors are contrast vectors as for the defect detector, and the output vectors are defined as *pixel depth* (expressed in mm). They showed a satisfied result for depth estimator.

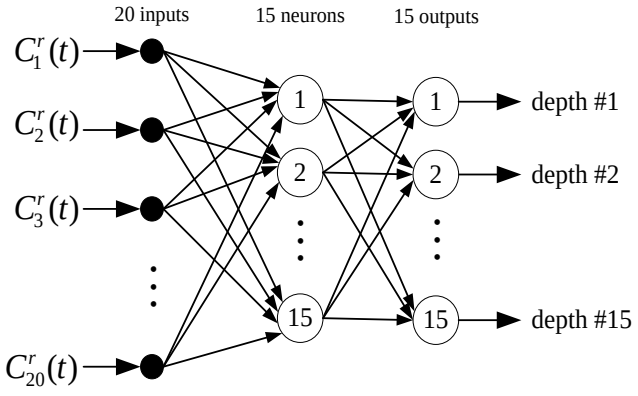

Figure 2.6 MLP-NN as depth estimator for CFRP material

Ludwig and Teruzzi (2002) proposed the modified version of using FWHM for defect sizing of the circular defect with low diffusivity materials by means of transient thermography. They showed that the lateral heat transfer influences the FWHM of the thermal contrast.

Dufour (2005) proposed one dimensional gradient for detecting defect edges in longitudinal and transversal direction. The edge gradients are $g(x) = T(x+1) - T(x-1)$ and $g(y) = T(y+1) - T(y-1)$ for transversal and longitudinal directions respectively, where T is the temperature value. The defect size in each direction is the distance between the maximum and the minimum gradients in that direction.

2.4 The Proposed Defect Characterization Technique

All the discussed techniques were devoted in the context of active thermography, except as proposed by Dufour (2005) in which this non-NN technique can be used for passive thermography application. It had been demonstrated in the previous reports that NN had been successfully applied for defect characterization in active thermography. Hence, this thesis is also motivated to use NN paradigm for defect characterization in passive thermography application.

The NN-based defect characterization for passive thermography is devoted for furnace wall application. Many models along with its defective refractory wall

are then built and with this data simulated using FEM. The MLP-NN is trained using the proposed informative parameters as the inputs and corresponding defect's depth as the outputs. For defect characterization of a test thermal image, the defect is detected with the proposed technique and localized using windowing technique. The informative parameters are then extracted and pass to the MLP-NN for characterization.

2.5 Summary

This chapter has discussed on the common modeling technique for infrared thermography application. Current research for defect characterizations is also elaborated. The trend in employing numerical modeling for thermography and its importance has been discussed in the chapter beginning. The proposed technique for defect depth estimation based on MLP-NN has been introduced briefly.

CHAPTER 3

ESTIMATING SPALLING DEFECT DEPTH

3.1 Introduction

Furnace linings may be single or multilayer form. Single layer usually suffices for furnaces operating at temperatures below 760^0C. Lining for modern high-temperature furnaces are almost always multilayer. The high temperature layer, which forms the interior surface of the refractory, referred to as 'hot-face', is backed by one or more layers of less-duty refractory and/or insulating materials, and finally the outer metal shell or 'skin' (cold-face) (Trinks et al, 2004). At temperatures above 2000^0F (1367^0C), refractories become more and more porous, allowing the hot furnace gases to attack the chemistry of the refractory. In time, this attack reduces the surface strength of the refractories and causes their melting temperature to be lowered (Trinks et al, 2004).

3.2 Spalling Defect

Griswold (1946) mentioned that the most common defect which occurred within refractory wall is the *spalling defect* which is the breaking or cracking of refractory brick in service, to such an extent those pieces are separated or fallen away, leaving new surfaces of the brick exposed. Since the crack or spalling defect within a refractory wall can cause heat losses to the external environment which can cause the furnace to unable to function at its optimum temperature, decrease in its efficiency, and increase in its operating cost. Therefore, the early sign of the defect existence should be known promptly. Jaeger (2000) proposed the impact-echo method while Maldague (2001) suggested infrared thermography (IRT) technique to assess the wall integrity. IRT uses the distribution of surface temperatures to assess the structure or behavior of what is under the surface. Thermal infrared camera is employed to record the temperature distribution which is called as *thermal image* or *thermogram* (Gaussorgues, 1994).

IRT has gained its popularity in the last few decades over other predictive maintenance techniques due to its many advantages. Being contactless, easy interpretation, large inspection coverage, and free from dangerous of radiation are among some of them. Above all, IRT has been successfully applied to solve many real world problems. Based on how the thermogram is produced, IRT has two approaches: *active thermography*, where an external heat source is needed to stimulate the materials to be inspected, and *passive thermography*, where external heat source is not needed, in which the test materials or structures are naturally already at a different (often higher) temperature than ambient.

3.3 Modeling of Spalling Defect

In IRT, numerical modeling is a precious tool, especially since it can provide limits to the effectiveness of the thermal nondestructive testing (TNDT) technique and also the possibility of considering different defect geometries and determining their detectability without the expense of making and testing the corresponding specimens (James et al, 1989). Other purpose of numerical modeling in IRT is to simulate the real situation in order to obtain the simulated thermogram from that simulation (Conner, 1998). This thermogram can later be used to test the developed algorithms (mainly related to image processing) in case of the unavailability of the thermogram from the real object, for instance due to the difficulties to obtain such thermal data.

From modeling tools perspective, there are two common methods for numerical modeling in IRT that are finite difference method (FDM) (Özişik, 1994; Croft and Lilley, 1977) and finite element method (FEM) (Segerlind, 1984; Rao, 1989). FDM is simple and easy to implement but it suffers when handling irregular geometry or anisotropic materials. FEM although is quite complex but it can work elegantly on deformed shape and non-homogeneous materials (ElShayeb and Beng, 2000), can improve accuracy and efficiency (Huebner et al, 1995).

Most common technique nowadays in IRT is application of FEM. Although in the early years FDM was usually employed for heat behavior study (Saintey and Almond, 1997), but in the last few years, the trend shows that FEM is common alternative used by researchers

(Krishnapillai et al, 2006). Hence, this report takes the advantage of FEM for modeling the spalling defect.

Consider a typical four layers furnace wall in Figure 3.1(a). The thermal properties of these layers are given in Table 3.1, where k is the thermal conductivy and ρ is the bulk density.

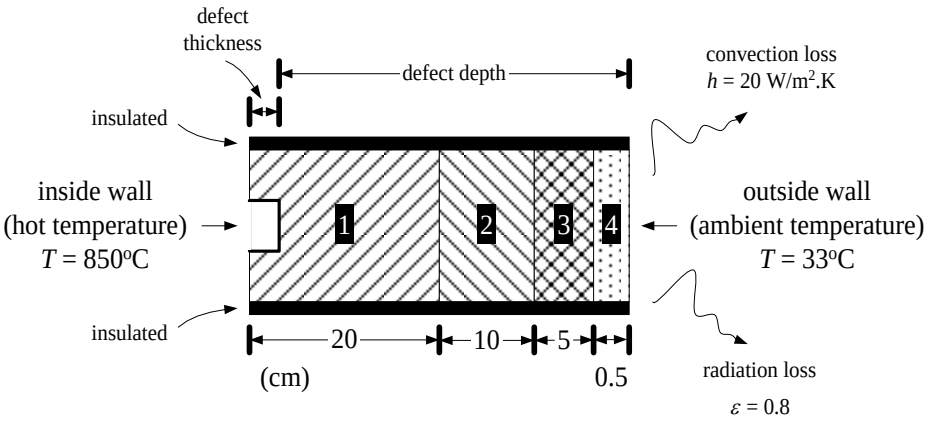

(a)

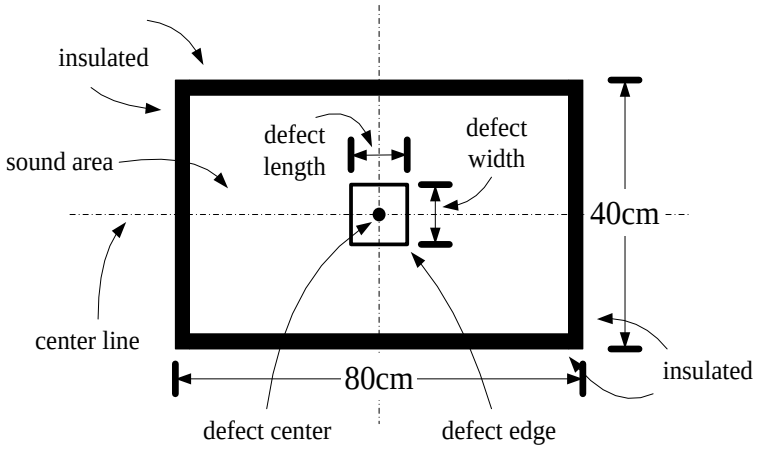

(b)

Figure 3.1: Typical four layers furnace wall: (a) side-view, and (b) front view

The spalling defect is simulated as a *void* occurred within refractory firebrick wall or the hot-face wall. The *defect depth* is defined as its depth from the outer wall (cold-face steel casing wall) or measured as the difference between the total lengths of the layered walls with the *defect thickness*. Figure 3.1(b) shows a portion of simulated wall with length of 80cm and width of 40cm. In this figure, the defect is located in the center of the wall model. Some terms introduced in this report are also shown in the figure.

Table 3.1: Thermal properties

Materials		k (W/m.K)	ρ (kg/m^3)
No.	**Name**		
1	Firebrick	1.436	2300
2	Insulation	0.225	1200
3	Fiber block	0.116	430
4	AISI 316 Steel	16.3	8000

In order to save the processing time, coarse elements were used in meshing process. Figure 3.2 shows the meshing result with 4cm element size of the modeled wall. Figure 3.3(a) shows the temperature distribution on the outer steel casing wall and Figure 3.3(b) shows the temperature distribution over the defect area along the center line of the wall. From this figures it is clear that due to the existence of the subsurface defect, an elevated temperatures are observed over the defect area as reflected on the outer surface wall. From the figure, the maximum temperature occurred on the center of the defect and gradually decreases near the defect edges.

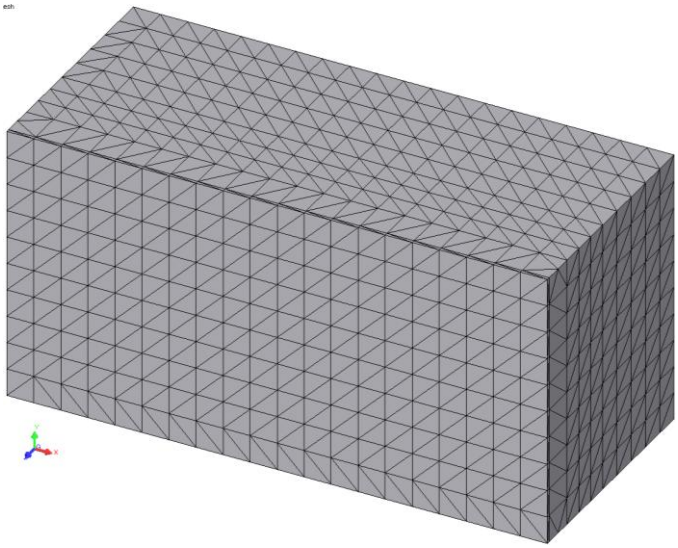

Figure 3.2: Model after meshing operation

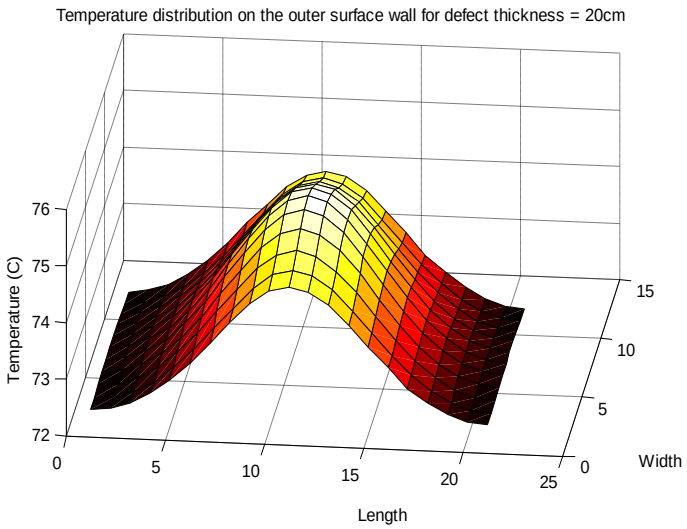

(a)

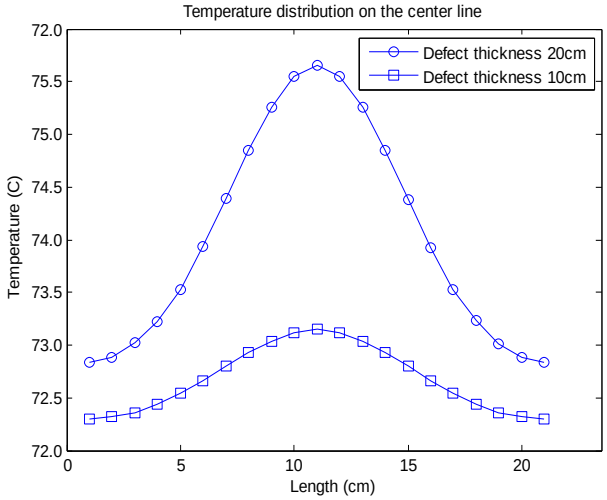

(b)

Figure 3.3: (a) Temperature distribution on the outer surface wall, (b) temperature distribution over the defect area along the center line of the wall for defect thickness 20cm and 10cm with defect size 15cm×15cm

3.4 Informative Parameters

Figure 3.3(b) clearly shows that temperature distributed on the outer wall surface has a relation with defect depth (thickness). It was also confirmed by the previous research (Heriansyah and Abu-Bakar, 2007) that there is strong interdependence between the defect depth and the *maximum temperature over the defect area* ($T_{max\text{-}def}$) as depicted in a thermal image of furnace wall.

If the spalling defect shape is uniform then due to the symmetry property of the finite element model, this maximum value will always be the peak value or at the defect center as

shown in Figure 3.3. Figure 3.4 shows the relationship between the defect depth and maximum temperature value within defect area. It is obvious that deeper the thickness of the defect or shallower the defect depth from the outer surface will increase the temperature value at that surface.

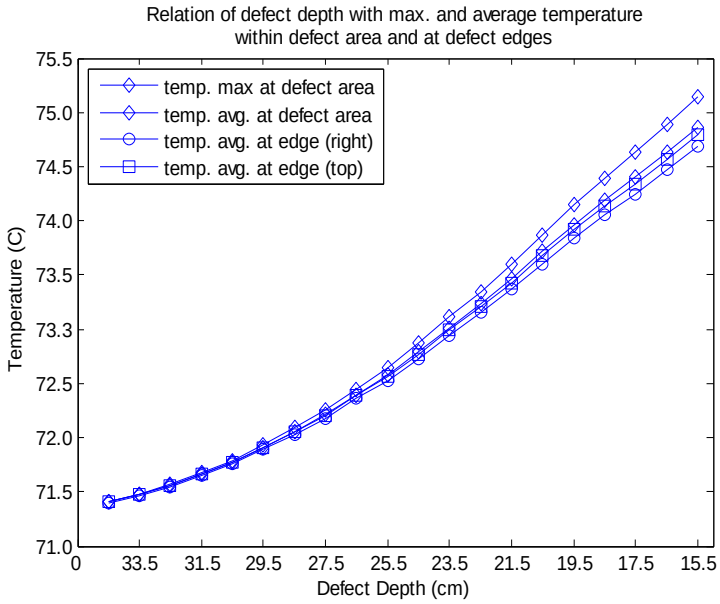

Figure 3.4: Relation of defect depth with maximum and average temperature within defect area and at right and top edges.

From Figure 3.3, it shows that from the peak, the temperature gradually decreases to the model edge. Therefore, at the defect edge (left, right, top, and bottom) the temperature is smaller than at the peak. Again, due to the symmetry property, for a uniform spalling at the left and right, and top and bottom of the defect edge will always have equal temperature values. Figure 3.4 shows the relation of defect depth with temperature at the right and top edge of the defect. In this report, the *average value of the right edge* ($T_{avg\text{-}right}$) and the *average value of the top edge* ($T_{avg\text{-}top}$) are used as the informative parameters.

As the temperature increases due to the defect depth, the *average temperature over defect area* ($T_{avg\text{-}def}$) reflected at the outer wall will also increase as shown in Figure 3.4. The same situation is also observed for the *average temperature on the sound* (non-defective) area ($T_{avg\text{-}so}$) as shown in Figure 3.5. These figures also illustrate that the relation between the defect depth and these informative parameters ($T_{max\text{-}def}$, $T_{avg\text{-}right}$, $T_{avg\text{-}top}$, $T_{avg\text{-}def}$, $T_{avg\text{-}so}$) tend to have a linear property. Note that all of these parameters were derived from a fix defect size and the defect is situated at the center of the wall model (Figure 3.1(b)).

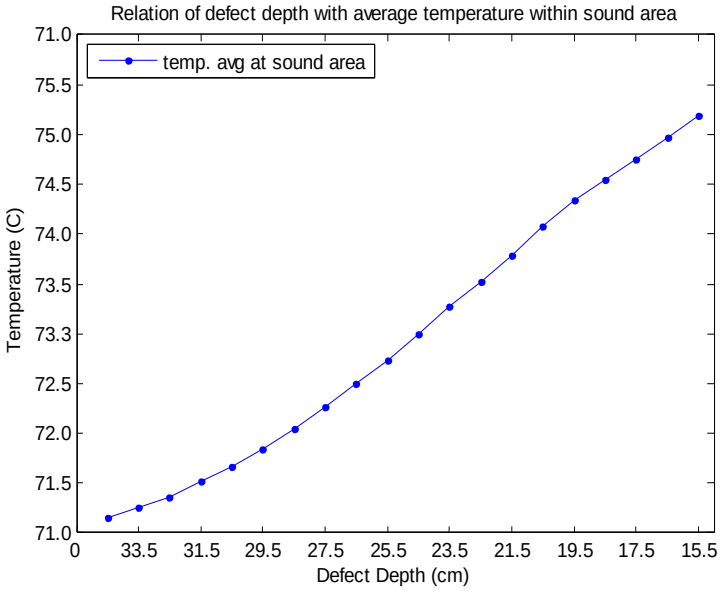

Figure 3.5: Relationship between the defect depth and average temperature within sound area.

Figure 3.6 shows the wall model with 15cm×15cm defect size and 20cm of defect thickness, and the defect is located at the *top-right corner* of the wall model. Figure 3.7 shows the temperature distribution at the outer surface wall and at the center line. It is clear that due to nonsymmetrical position of the spalling defect, the temperature distribution reflected at the outer surface wall is nonsymmetrical as well. Another fact also confirmed that elevated temperatures occurred over the defect area and defect depth has relation with temperature values. The temperature increases as the defect depth decreases (or defect thickness increases).

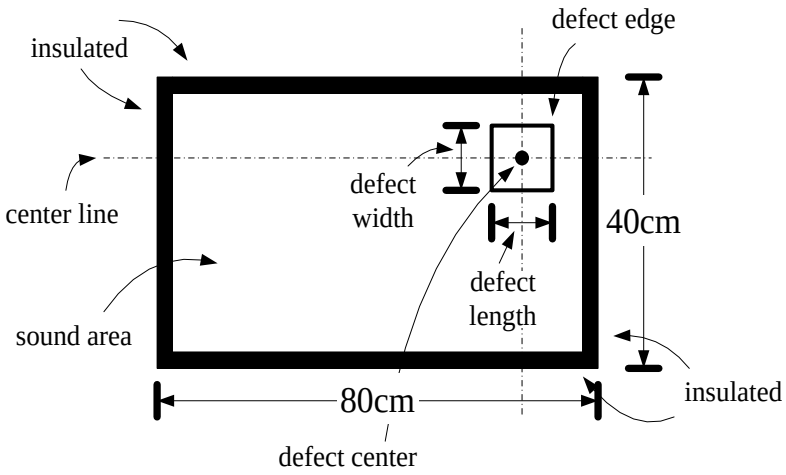

Figure 3.4: Front view of spalling defect located at the top-right corner of the wall model.

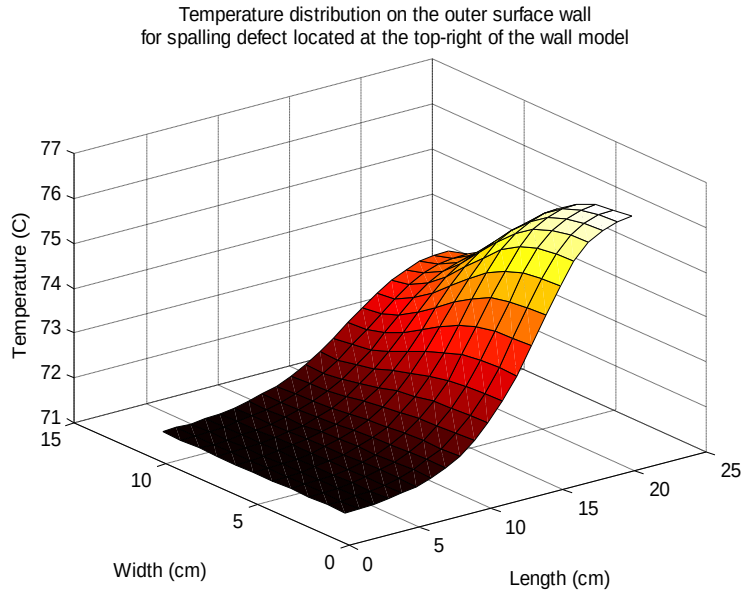

(a)

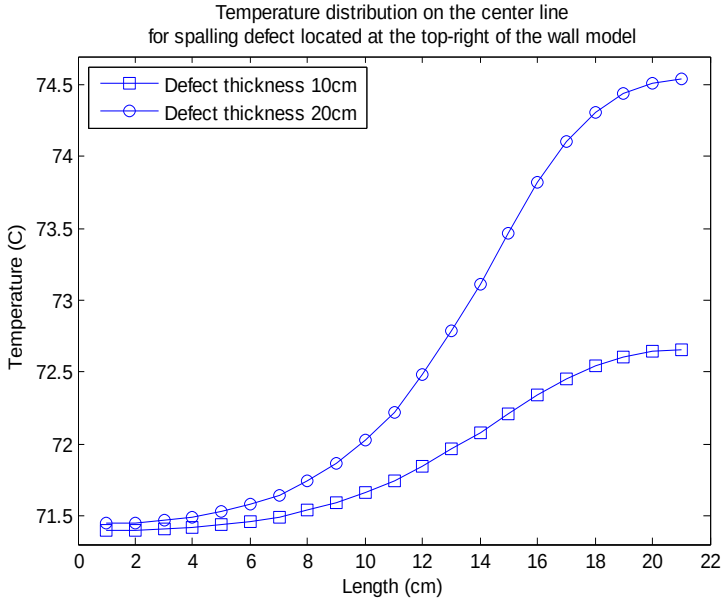

(b)

Figure 3.5: (a) Temperature distribution on the outer surface wall for the spalling defect located at the top-right corner of the wall model, (b) temperature distribution over the defect area along the center line of the wall for defect thickness 20cm and 10cm with defect size 15cm×15cm.

3.5 Depth Estimator

Artificial neural network (ANN) is a simple abstraction of biological neurons. Networks of these artificial neurons do not have a fraction of the power of the human brain, but they can be trained to perform useful functions (Hagan et al, 1996).

In recent years many researchers have used ANN to solve complex nonlinear real world problems. ANNs are potentially powerful, robust and adaptive tools for detecting and classifying targets under changing signature or environmental conditions (Darabi and Maldague, 2002). These capabilities have motivated some researchers to employ ANN to solve their thermography problems. Saintey and Almond (1997), used finite difference modeling to generate input training data for neural network interpreter to determine defect size and depth. Darabi and Maldague (2002), did a similar approach in which they used three dimensional heat transfer models to generate synthetic data to train neural network depth estimator by means of active thermography. All existing depth estimation based on ANN (Saintey and Almond, 1997; Darabi and Maldague, 2002; Maldague et al, 1998; Manduchi et al, 1997; Vallerand and Maldague, 2000; D'Orazio et al, 2005) were designed for active thermography application. This report uses numerical method to simulate the spalling defect behavior in term of temperature distribution and to employ this simulated as the input parameters to train ANN for defect depth estimation in a passive thermography scheme.

In this report, a *multilayer perceptrons* (MLP) and *radial basis function* (RBF) neural networks were trained to have the capability in the estimation of defect depth which may occur within the furnace refractory. MLP was selected as depth estimator since it is a common ANN paradigm used for various applications with satisfactory results (Jain and Fanelli, 2000). While, RBF was selected as the comparator, actually is not really 'to compare' but as an alternative way when using ANN approach for this specific application.

As already shown in the previous section, the maximum temperature over the defect area ($T_{max\text{-}def}$), the average temperature at the right edge ($T_{avg\text{-}right}$), the average temperature at the top edge ($T_{avg\text{-}top}$), the average temperature within defect area ($T_{avg\text{-}def}$), and the average temperature within the sound area ($T_{avg\text{-}so}$) are indeed related to the spalling defect depth. Therefore, these five parameters are employed in the ANN training for spalling depth

estimation. These parameters are extracted from the numerical modeling as discussed in the previous section.

For the training purpose, the following defect depths are used: 34.5, 33.5, 32.5, 31.5, 30.5, 29.5, 28.5, 27.5, 26.5, 25.5, 24.5, 23.5, 22.5, 21.5, 20.5, 19.5, 18.5, 17.5, 16.5, and 15.5 cm. Again, note that defect depth in our case is measured from the outer face (steel) wall (refer to Figure 3.1(a)).

3.5.1 Multilayer Perceptrons

Multilayer feedforward networks (or commonly referred as *multilayer perceptrons*) is one of important class of neural networks. It consists of a set of sensory units (source nodes) that constitute the *input layer*, one or more *hidden layers* of computation nodes, and an *output layer* of computation nodes (Haykin, 1994). Figure 3.8 shows the architecture of an MLP network. Popular algorithm to train an MLP network is *back propagation* algorithm.

Each nodes connected by a quantity called *weights*. The basic purpose of training a network is to optimize weights corresponding to a particular set of input-output training patterns. The response at a node is calculated by evaluating the contributions from all the input nodes through a nonlinear mapping function.

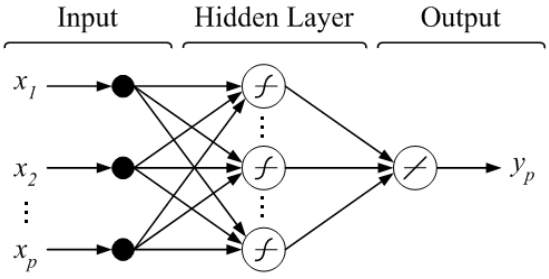

Figure 3.6: MLP network

3.5.2 Radial Basis Function

The construction of an RBF network in its most basic form involves three entirely different layers. The *input layer* is made up of source nodes (sensory units). The second layer is a *hidden layer* of high enough dimension, which serves a different purpose from that in a

MLP. The *output layer* supplies the response of the network to the activation patterns applied to the input layer. The transformation function from the input space to the hidden-unit space is *nonlinear* (Gaussian), whereas *linear* for hidden-unit space to the output (Haykin, 1994; Demuth and Beale, 2001). Figure 3.9 shows the architecture of a RBF network.

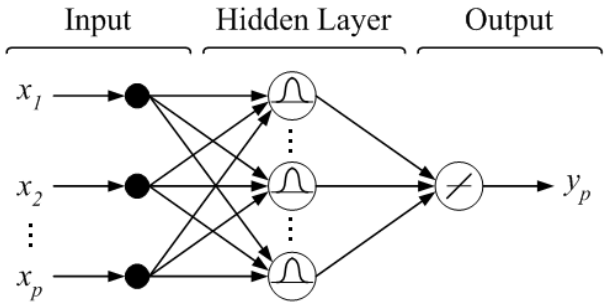

Figure 3.7: RBF network

CHAPTER 4

RESULTS AND DISCUSSION

4.1 Overview

In this chapter, results of depth estimation from using two classifiers as proposed in Chapter 3 (MLP and RBF) will be presented. For the purpose of training, 20 defect samples of different depths (mentioned in Chapter 3) were employed. The size of the defect was set to 15cm x 15 cm. The defect samples were simulated using SolidWorks and COSMOSworks software packages. The parameters for the layers are as mentioned in Chapter 3.

4.2 Experiments with Multi Layer Perceptron and Radial Basis Function

The input data for training are $T_{max\text{-}def}$, $T_{avg\text{-}right}$, $T_{avg\text{-}top}$, $T_{avg\text{-}def}$ and $T_{avg\text{-}so}$ and the corresponding values of defect depth were used as the outputs. One hidden layer with eight nodes of MLP was found to be effective for this purpose. The parameters used for training were 0.04 for learning rate, 0.9 for momentum, and 1×10^{-03} for error rate. Figure 4.1 shows the defect depth estimation results by both networks for the trained data as compared to the actual depth. Errors for depth estimation in both cases were found to be zero, or 100% correct estimation.

Figure 4.2 shows the depth estimation for untrained data (of depth 35, 34, 33, 32, 31, 30, 29, 28, 27, 26, 25, 24, 23, 22, 21, 20, 19, 18, 17, and 16cm respectively from the outer surface wall). Depth estimation error for this untrained data is shown in Table 4.1 for MLP and in Table 4.2 for RBF network result.

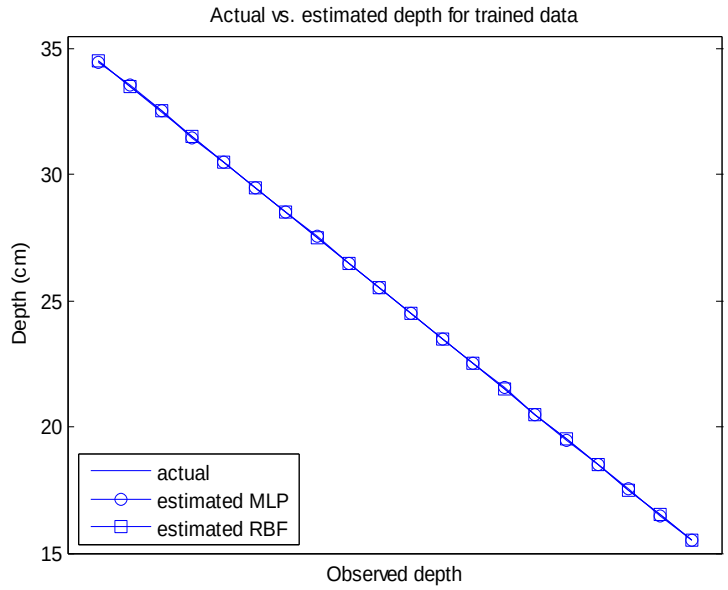

Figure 4.1: Estimated depth for trained data

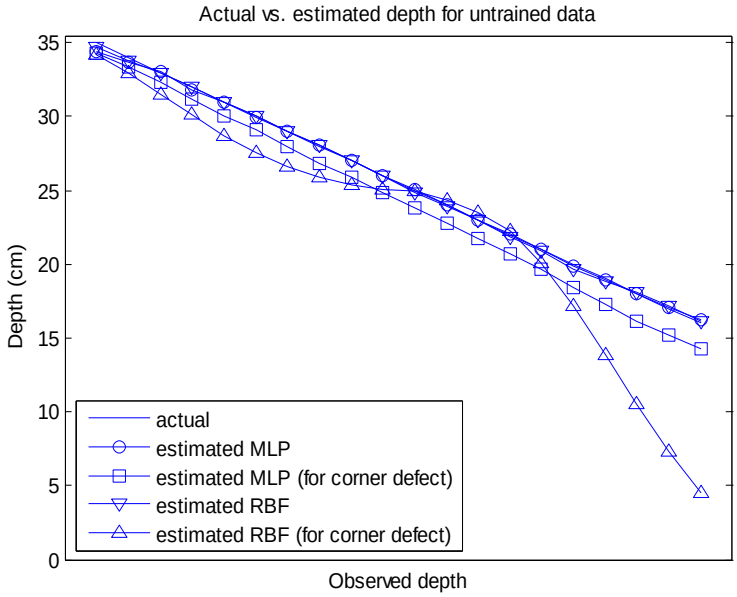

Figure 4.2: Estimated depth for untrained data

From Table 4.2, for the case of *center spalling* defect (Center), there is no depth estimation error for all defects except for defect with depth 35cm, the error is around 2.86%. MLP can estimate correctly without error for 19 depths (34 to 16cm). For the case of *top-right corner spalling* defect (Corner), all errors are no more than 12.50% or even for the worst case, the accuracy is still around 87.50%. In which, 15 depths (35 to 21cm) have error less than 5% (95% accuracy), and 5 depths (20 to 16cm) have error less than 13% (87%

accuracy). The average error for center spalling is 0.14% (99.86% accuracy), and the average error for top-right corner spalling is 5.54% (94.46% accuracy).

Table 4.1: Depth estimation error for untrained data of MLP networks

Actual Depth	Estimated Depth		Error (%)	
	Center	Corner	Center	Corner
35	34	34	2.86	2.86
34	34	33	0	2.94
33	33	32	0	3.03
32	32	31	0	3.13
31	31	30	0	3.23
30	30	29	0	3.33
29	29	28	0	3.45
28	28	27	0	3.57
27	27	26	0	3.70
26	26	25	0	3.85
25	25	24	0	4.00
24	24	23	0	4.17
23	23	22	0	4.35
22	22	21	0	4.55
21	21	20	0	4.76
20	20	18	0	10.00
19	19	17	0	10.53
18	18	16	0	11.11
17	17	15	0	11.76
16	16	14	0	12.50

Table 4.2: Depth estimation error for untrained data of RBF networks

Actual Depth	Estimated Depth		Error (%)	
	Center	Corner	Center	Corner
35	35	34	0	2.86
34	34	33	0	2.94
33	33	31	0	6.06
32	32	30	0	6.25
31	31	29	0	6.45
30	30	28	0	6.67
29	29	27	0	6.90
28	28	26	0	7.14
27	27	25	0	7.41
26	26	25	0	3.85
25	25	25	0	0.00
24	24	24	0	0.00
23	23	24	0	-4.35
22	22	22	0	0.00
21	21	20	0	4.76
20	20	17	0	15.00
19	19	14	0	26.32
18	18	11	0	38.89
17	17	7	0	58.82
16	16	5	0	68.75

From Table 4.2, for the case of *center spalling* defect, RBF can estimate correctly for all defect depths without error. For *top-right corner spalling*, the worst estimation is for 16cm depth, the error is greater than 60%. The next worst are in estimating 17cm and 18cm depths, with errors greater than 50% and 30% respectively. Other depths estimation is all under 30% error (70% accuracy). Hence, the average error for center defect is 0% (100% accuracy), and 13.27% (86.73% accuracy) for the case of top-right corner defect.

CHAPTER 5

CONCLUSIONS AND FUTURE WORK

5.1 Summary and Conclusion

In Chapter 1, the introduction on infrared thermography (IRT) and its applications in petrochemical industry was described. In conjunction with this, several types of refractory were discussed. In similar manner the concept of how the heat was loss was briefly described. In addition, the scope and objective of the project were properly stated.

In Chapter 2, review on several techniques in modeling defects and defect characterization were presented. Two common types in numerical modeling namely finite difference method and finite element method were presented. Advantages and disadvantages of these algorithms were addressed. A brief introduction of the proposed technique is given in the end of the chapter.

Chapter 3 described the complete process of modeling the furnace with actual parameter values. In is also in this chapter that the relationship between the defect depth and five temperature values was established. These temperature values were later used as input to the neural network paradigm for estimating the depth. In doing so two types of artificial neural network (ANN) systems were proposed – multi layer perceptron and radial basis function systems.

In Chapter 4, experimental results showed the effectiveness of the proposed algorithms. Twenty defect depths were used training the ANN and another set of twenty defect depths were used for performance evaluation. The results for both ANN systems showed very promising performance. Performance based on different locations of the defect was also investigated and the results showed a slight degradation in performance for defects situated at the corner of the furnace.

It has been shown from the result in the previous section that the depth estimation by using MLP and RBF neural networks paradigm both for trained and untrained data is quite satisfactory. There is no estimation error for both networks for trained data. The average error for untrained data for MLP is less than 1% for the case of center defect, and less than 6% for the case of top-right corner defect. The average error for RBF is 0% for the case of center defect, and less than 14% for the case of top-right corner defect.

It is shown that the average error for RBF is quite greater than MLP for the case of top-right corner spalling, but it can estimate correctly for all depths for the case of center spalling type defect. Therefore as the rule of thumb, we can say generally that in this specific application MLP is better than RBF for both cases. Even with the lack of training data and quite different testing data, MLP still can give proper estimation results.

The results showed us that the informative parameters ($T_{max\text{-}def}$, $T_{avg\text{-}right}$, $T_{avg\text{-}top}$, $T_{avg\text{-}def}$ and $T_{avg\text{-}so}$) proposed in this paper are suitable for depth estimation in passive thermography. As already shown in previous section, these informative parameters have a relationship with spalling defect depth. Although these informative parameters will give a slightly different values for different spalling defect location in the model (as shown in Figure 7), but still with these five parameters, ANN give a satisfactorily results for trained and untrained data for both networks.

5.2 Suggestions for Future Research

For the future works, other informative parameters can be explored, moreover to preserve the spalling defect location property and ANN can be trained with more input data to achieve a better generalization.

Neural network paradigm with its ability to learn and adapt to a new pattern has a great potential for the estimation of the defect depth. This paper has demonstrated on how to employ ANN paradigm for depth estimation in a passive thermography. Two NN paradigms: MLP and RBF networks have been employed and the results are promising.

REFERENCES

Akin, J. E. (2005). *Finite Element Analysis with Error Estimators.* Oxford: Elsevier Butterworth-Heinemann.

Almond, D. P. and Lau, S. K. (1994). Defect Sizing by Transient Thermography I: An Analytical Treatment. *J. Phys. D: Appl. Phys.* 27: 1063-1069.

Andreev, K. and Harmuth, H. (2003). FEM Simulation of the Thermo-Mechanical Behavior and Failure of Refractories – A Case Study. *Journal of Materials Processing Technology.* 143-144: 72-77.

Bonin, R. G. (2003). IR Applications for Process Vessels. *Proceedings of InfraMation 2003.* Las Vegas, Nevada. Oct. 13-16, 2003.

Buglia, J. J. and Brinkworth, H. (1958). A Comparison of Two Methods for Calculating Transient Temperatures for Thick Walls. *NACA Technical Note 4343.*

Carniglia, S. A. and Barna, G. L. (1992). *Handbook of Industrial Refractories Technology: Principles, Types, Properties, and Applications.* Noyes Publications.

Chanda, B. and Majumder, D. D. (2000). *Digital Image Processing and Analysis*. New Delhi: Prentice-Hall of India Private Limited.

Charles, J. A. and Wilson, D. W. (1980). A Model of Passive Thermal Nondestructive Evaluation of Composite Laminates. University of Delaware.

Chesters, J. H. (1973). *Refractories: Production and Properties.* The Iron and Steel Institute.

Chowdhury, R. (2004). Active Infrared (IR) Thermographic Testing Procedures by 3-D Finite Element Analysis and Experimental Correlations. Wayne State University, USA: M.Sc Thesis.

Cone, C. (1980). *Energy Management for Industrial Furnaces.* John Wiley & Sons, Inc.

Conner, C. D. (1998). Thermographic Defect Detection and Classification from Noisy Infra-red Image Sequences. The Catholic University of America: Ph.D Thesis.

Croft, D. R. and Lilley, D. G. (1977). *Heat Transfer Calcultions using Finite Difference Equations.* Applied Science Publishers, Ltd.

D'Orazio, T., Guaragnella, C., Leo, M., and Spagnolo, P. (2005). Defect Detection in Aircraft Composites by using a Neural Approach in the Analysis of Thermographic Images. *NDT&E International.* 38: 665-673.

Darabi, A. (2000). Detection and Estimation of Defect Depth in Infrared Thermography using Artificial Neural Networks and Fuzzy Logic. Université Laval, Canada: Ph.D Thesis.

Darabi, A. and Maldague, X. (2002). Neural Network based Defect Detection and Depth Estimation in TNDE. *NDT&E International.* 35: 165-175.

Demuth, H., Beale, M., and Hagan, M. (2008). *Neural Network Toolbox™ 6: User's Guide*. Natick, MA: The MathWorks, Inc.

Doležal, R. (1961). *Large Boiler Furnaces: Theory, Construction and Control.* Elsevier Publishing Company.

Dufour, M. B. (2005). Quantification of Air Leaks through the Building Envelope using Infrared Thermography. Concordia University, Canada: M.Ap.Sc Thesis.

ElShayeb, M. and Beng, Y. K. (2000). *Application of Finite Difference and Finite Element Methods for Thermal Problems.* Sabah, Malaysia: Universiti Malaysia Sabah.

Gardner, W. E. (1992). *Improving the Effectivenes and Reliability of Non-destructive Testing.* Oxford, England: Pergamon Press, Ltd.

Gaussorgues, G. (1994). *Infrared Thermography.* Cambridge: Chapman & Hall.

Ghojel, J. I. and Ibrahim, R. N. (2004). Computer Simulation of the Thermal Regim of Double-loop Channel Induction Furnaces. *Journal of Materials Processing Technology.* 155-156: 2093-2098.

Griswold, J. (1946). *Fuels, Combustion, and Furnaces*. McGraw-Hill Book Company, Inc.

Gruber, D., Andreev, K., and Harmuth, H. (2004). FEM Simulation of the Thermomechanical Behaviour of the Refractory Lining of a Blast Furnace. *Journal of Materials Processing Technology.* 155-156: 1539-1543.

Haykin, S. 1994. *Neural Networks: A Comprehensive Foundation*. NY: Macmillan College Publishing Company, Inc.

Huebner, K. H., Thornton, E. A., and Byrom, T. G. (1995). *The Finite Element Method for Engineers*. 3rd ed. Canada: John Wiley & Sons, Inc.

Jain, L. and Fanelli, A. M. (2000). Recent Advances in Artificial Neural Networks: Design and Applications. Boca Raton: CRC Press LLC.

James, P. H., Welch, C. S., and Winfree, W. P. (1989). A Numerical Grid Generation Scheme for Thermal Stimulation in Laminated Structures. In Thompson, D. E. and Chimneti, D. E. eds. *Review of Progress in Quantitative Nondestructive Evaluation.* 8A: 801-809.

Kaplan, H. (1993). *Practical Applications of Infrared Thermal Sensing and Imaging Equipment.* Bellingham, Washington: SPIE-The International Society for Optical Engineering.

Kattan, P. I. (2003). *MATLAB Guide to Finite Elements: An Interactive Approach.* Germany: Springer-Verlag Berlin Heidelberg.

Krishnapillai, M., Jones, R., Marshal, I. H., Bannister, M., and Rajic, N. Thermography as a Tool for Damage Assessment. (2005). *Composite Structures.* 67: 149-155.

Krishnapillai, M., Jones, R., Marshall, I. H., Bannister, M., and Rajic, N. (2006). NDTE using Pulse Thermography: Numerical Modeling of Composite Subsurface Defects. *Composite Structures.* 75: 241-249.

Kurowski, P. M. (2006). *Engineering Analysis with COSMOSWorks Professional 2006.* SDC Publishing.

LeClercq, A. J. (2003). The Art of Furnace Tube Skin Temperatur Analysis. *Proceedings of InfraMation 2003.*

Levitt, J. (2003). *Complete Guide to Preventive and Predictive Maintenance.* New York: Industrial Press, Inc.

Lewis, R. W., Nithiarasu, P., and Seetharamu, K. N. (2004). *Fundamentals of the Finite Element Method for Heat and Fluid Flow.* West Sussex, England: John Wiley & Sons Ltd.

Lo, T. Y. and Choi, K. T. W. (2004). Building Defects Diagnosis by Infrared Thermography. *Structural Survey.* 22(5): 259-263.

Ludwig, N. and Teruzzi, P. (2002). Heat Losses and 3D Difussion Phenomena for Defect Sizing Procedures in Video Pulse Thermography. *Infrared Physics & Technology*. 43: 297-301.

Maierhofer, Ch., Wiggenhauser, H., Brink, A., and Röllig, M. (2004). Quantitative Numerical Analysis of Transient IR-experiments on Buildings. *Infrared Physics & Technology*. 46: 173-180.

Maldague, X. P. V. (1993). *Nondestructive Evaluation of Materials by Infrared Thermography.* Springer-Verlag London Limited.

Maldague, X. P. V. (2001). *Theory and Practice of Infrared Technology for Nondestructive Testing.* John Wiley & Sons, Inc.

Maldague, X., Largouët, Y, and Couturier, J. P. (1998). A Study of Defect Depth using Neural Networks in Pulsed Phase Thermography: Modelling, Noise, Experiments. *Rev. Gén. Therm.* 37: 704-717.

May, K. B. (2003). Predictive Maintenance Inspections – Boilers in Fossil Power Plants. *Proceedings of InfraMation 2003.*

Mobley, R. K. (1990). *An Introduction to Predictive Maintenance*. New York: Van Nostrand Reinhold.

MTBE Sdn. Bhd. (2007). *Thermography Scanning Report*. Oct. 24, 2007. Kuantan, Pahang.

Nyholt, J. J. (2000). Infrared Thermography in BP Amoco – Petrochemical Applications. *Proceedings of InfraMation 2000.*

Ohliger, A. A. (2002). Using Infrared Thermography on Offshore Platform Equipment. *Proceedings of InfraMation 2004.*

Ohliger, A. A. (2003). Horsehead (beam) pump Infrared Analysis. *Proceedings of InfraMation 2003.*

Ohliger, A. A. O. and Alvarado, G. E. (2001). Texaco's Use of Infrared on Fired Process Heaters. *Proceedings of InfraMation 2001.*

Özişik, M. N. (1994). *Finite Difference Methods in Heat Transfer*. CRC Press, Inc.

Plotnikov, Y. A. (1998). Modeling of the Multiparameter Inverse Task of Transient Thermography. *Proceedings of the 25th Annual Review of Progress in Quantitative Nondestructive Evaluation Conference.* Snowbird, Utah: Jul. 19-24, 1998. 873-880.

Plotnikov, Y. A. and Winfree, W. P. (2000). Temporal Treatment of a Thermal Response for Defect Depth Estimation. In Thompson, D. O. and Chimenti, D. E. eds. *Review of Progress in QNDE*. 19. AIP.

Qi, H., Kuruganti, P. T., and Liu, Z. (2002). Early Detection of Breast Cancer using Thermal Texture Maps. *Proceedings of IEEE.* 309-312.

Rao, S. S. (1989). *The Finite Element Method in Engineering.* 2nd ed. Oxford, England: Pergamon Press plc.

Sabir, A. B. and Mousa, A. I. (1999). The Analysis of Storage Tanks by the Finite Element Method. *Computatinal Structural Engineering for Practice.* 189-196.

Saintey, M. B. and Almond, D. P. (1995). Defect Sizing by Transient Thermography II: A Numerical Treatment. *J. Phys. D: Appl. Phys.* 28: 2539-2546.

Saintey, M. B. and Almond, D. P. (1997). An Artificial Neural Network Interpreter for Transient Thermography Data. *NDT&E International.* 30(5): 291-295.

Segerlind, L. J. (1984). *Applied Finite Element Analysis.* 2nd ed. John Wiley & Sons, Inc.

Sims, D. L. (2001). Using Infrared Imaging on Production Tanks & Vessels. *Proceedings of InfraMation 2001*.

SRAC (Structural Research and Analysis Corporation). (2004). *Introducing COSMOSWorks.* LA, California.

Sukirman, Y. (1994). A Finite Element Solution for Solving a Fully Coupled Problem in Petroleum Reservoir Engineering. *Proceedings of Seminar Sains Matematik dalam Industri.* Dec. 27-29, 1994. Skudai, Johor. 1-12.

Trinks, W., Mahinney, M. H., Shannon, R. A., Reed, R. J., and Garvey, J. R. (2004). *Industrial Furnaces.* 6th ed. John Wiley & Sons, Inc.

Vallerand, S. and Maldague, X. (2000). Defect Characterization in Pulsed Thermography: A Statistical Method Compared with Kohonen and Perceptron Neural Networks. *NDT&E International.* 33: 307-315.

Wang, W., Zeng, Y., Ma, D., Jin, Z., Wu, H., Yuan, C., and Yuan, Y. (2004). Clinical Study on using Thermal Texture Maps in SARS diagnosis. *Proceedings of the 26th Annual International Conference of the IEEE EMBS*. 5258-5264.

Weigle, R. K. (2005). Applications of Infrared Thermography for Petrochemical Process Heaters. *Proceedings of the SPIE Thermosense XXVII.* 5782: 100-108.

Whitcher, A. (2003). Thermographic Monitoring of Refractory Lined Petroleum Refinery Equipment. *Proceedings of InfraMation 2004.*

Willis, J. (2004). Lagged Pipe Survey. *Proceedings of InfraMation 2004.*

PUBLICATION

1. Rudi Heriansyah and S. A. R. Abu-Bakar. "Simulating and Estimating Spalling Defect Depth in Passive Thermography using Neural Network Techniques". *Special Issue on Advances in Mechatronics and AI Models, International Journal of Simulation: Systems, Science, and Technology* (IJSST), United Kingdom Simulation Society, Vol. 9 (2): pp. 23-30, May 2008.

2. Rudi Heriansyah and S. A. R. Abu-Bakar. "Defect Depth Estimation in Passive Thermography using Neural Network Paradigm." *The 6th WSEAS International Conference on Circuits, Systems, Electronics, Controls & Signal Processing 2007* (*CSECS '07*), pages 421 – 425. Cairo, Egypt. Dec. 29-31, 2007.

3. Rudi Heriansyah and S. A. R. Abu-Bakar. "Defect Detection in Thermal Image using Thresholding Technique" *The 6th WSEAS International Conference on Circuits, Systems, Electronics, Controls & Signal Processing 2007* (*CSECS '07*), pages 341 – 346, Cairo, Egypt, Dec. 29-31, 2007.

4. Rudi Heriansyah and S. A. R. Abu-Bakar. "Defect Depth Estimation in Passive Thermography - Comparing Multilayer Perceptrons with Radial Basis Functions Networks." *Malaysia-Japan International Symposium on Advanced Technology 2007* (*MJISAT 2007*), Kuala Lumpur, Malaysia, Nov. 16-19, 2007.

5. Rudi Heriansyah and S. A. R. Abu-Bakar. "Modeling of Defects within High Temperature Wall by Means of Infrared Thermography." *International Conference on Risk Technology & Management 2007* (*RISKTech 2007*), pp 298-302, Bandung, Indonesia, Mar. 20-22, 2007.

6. Rudi Heriansyah, S.A.R. Abu-Bakar, "Defect Detection in Thermal Image for Nondestructive Evaluation of Petrochemical Equipments". *Journal of Non Destructive Testing & Evaluation* (*NDT&E*), June 21, 2009 (online) (Impact Factor 1.198).